Bulletin of the New Zealand Society for Earthquake Engineering, Vol. 49, No. 3, September 2016

EQUIVALENT FRAME MODELLING OF AN UNREINFORCED MASONRY BUILDING WITH FLEXIBLE DIAPHRAGMS – A CASE STUDY

Yasuto Nakamura[1], Hossein Derakhshan[2], Abdul H. Sheikh[3], Jason M. Ingham[4] and Michael C. Griffith[5]

(Submitted *January 2016*; Reviewed *March 2016*; Accepted *May 2016*)

ABSTRACT

A case study was conducted to investigate the applicability of the equivalent frame modelling for the nonlinear time-history analysis of unreinforced masonry buildings with flexible diaphragms. The dynamic responses calculated from the equivalent frame models were compared against shake table test results of a full-scale two-storey stone masonry building. The investigated modelling approach reflected the simplifications commonly assumed for the global analysis of buildings; namely, considering the diaphragms to behave elastically and neglecting the stiffness and strength contributions of the out-of-plane responding walls. The sensitivity of the analysis to different idealisations of the equivalent frame, as well as to the diaphragm stiffness values, were also investigated. Discussions are provided on the accuracies and limitations of the investigated modelling approach, which may serve as a useful guidance for practical application.

INTRODUCTION

Unreinforced masonry (URM) buildings make up a substantial proportion of existing building stock, and continue to pose large seismic risk in many parts of the world. In evaluating their seismic vulnerability, efficient numerical models are required, that are capable of simulating the inelastic building behaviour. The equivalent frame modelling procedure [1] has been shown to be a promising practical approach capable of simulating the salient response mechanisms of URM buildings, without incurring the large computational penalty of finite element analysis.

The equivalent frame idealisation considers the in-plane response of a wall as comprising of deformable pier and spandrel elements connected to nodes, which may have rigid offsets (Figure 1(a)). The minimum deformable length of the piers (spandrels) is commonly assumed to be dictated by the smallest height (width) of adjacent openings. Alternatively, to account for the deformability of the node panels, the deformable length of piers may be extended making use of 30° lines emanating from the corners of the door or window openings as shown in Figure 1(a). The piers and spandrels are conceptually represented as elastic frame members with lumped nonlinearity capturing the shear or rocking failure modes (Figure 1(b)). The initial validation of the equivalent frame modelling procedure was focused on individual in-plane loaded walls in isolation [1-3].

Subsequent developments have explored the feasibility of modelling the global three-dimensional response of buildings by assembling two-dimensional equivalent frames coupled by diaphragms [4].

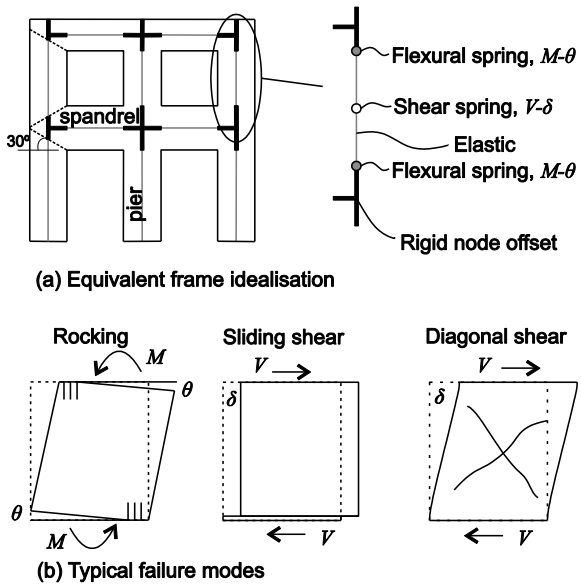

Figure 1: Equivalent frame idealisation and typical failure modes.

In such three-dimensional models, floor and roof diaphragms are often treated as stiffness contributing elements but do not have dynamic or vibration characteristics [4]. However, it is well recognised that the in-plane motions of flexible timber diaphragms, which commonly exist in URM buildings, can dominate the response of these buildings. This recognition is reflected in some guidelines [5] where the natural frequency of a building is considered to be approximately equal to the frequency of the diaphragm itself. Measurements taken from an instrumented URM building with timber diaphragms during the Loma Prieta earthquake [6] showed that the flexible diaphragms have the tendency of vibrating almost independently of the supporting walls, with amplified

[1] *Corresponding Author, PhD Candidate, University of Adelaide, Adelaide, yanakamura@pb.com.au*
[2] *Research Associate, University of Adelaide, Adelaide*
[3] *Associate Professor, University of Adelaide, Adelaide*
[4] *Professor, University of Auckland, Auckland*
[5] *Professor, University of Adelaide, Adelaide*

displacements and accelerations at their mid-spans. Similar behaviours were also observed in shake table tests by Costely and Abrams [7]. Evidence of significant diaphragm deformation was also found in at least one building during the 22 February 2011 Christchurch earthquake [8] where excessive in-plane diaphragm deformation was believed to have led to the out-of-plane collapse of a wall (Figure 2).

Figure 2: Out-of-plane wall failure caused by excessive diaphragm deformation [8].

Despite the importance of the dynamic characteristics of flexible diaphragms, the accuracy of an equivalent frame analysis incorporating such behaviour has not been investigated in detail so far. A notable exception is found in a recent study undertaken by Aleman et al. [9] who developed a numerical model of a typology of URM buildings commonly found in New York City. In their model, the in-plane walls were represented by equivalent frames and the timber floor joists and sheathing were represented as elastic beam elements that were connected through nonlinear springs to capture nail-slip behaviour, together with calibrated rotational springs representing the one-way vertically spanning out-of-plane loaded walls.

Such detailed nonlinear modelling, however, poses several problems in practice. The modelling of a timber diaphragm requires an individual nail force-slip relationship, which is typically not available in seismic codes and guidelines. The actual nonlinear behaviour of diaphragms also depends on the specific locations of the nail connections and on the spacing of the nail couple, which may be difficult to capture. The inclusion of one-way vertical bending corresponding to the out-of-plane deformation of walls, as done in [9], increases computational demand but does not necessarily enhance the analysis accuracy; recent research [10] has suggested that even for one-way (vertically) spanning wall modelling, an additional failure mode needs to be considered due to diaphragm flexibility. Such detailed modelling for the out-of-plane loaded wall is considered to be impractical.

The aim of this paper is to explore the applicability of the equivalent frame modelling approach for the prediction of global response of URM buildings with flexible diaphragms, considering the above limitations currently faced by practising engineers. To this end, a relatively simple modelling approach based on commonly accepted assumptions is investigated. Specifically, the diaphragms are represented by elastic membrane elements, while the out-of-plane wall stiffness and strength contributions are neglected. Dynamic test data of a full-scale stone masonry building with strengthened timber floor and roof [11] is used to verify the potential, and to identify the limitations, of the modelling approach. The sensitivity of the analysis for different choices of modelling are also explored through two different equivalent frame idealisations and diaphragm stiffness values. While the analyses are conducted using TREMURI [4] with certain modelling concepts specific to that program, results reported in this paper have general applicability.

CASE STUDY BUILDING

A two-storey stone masonry building with a timber floor and a timber roof diaphragm tested at EUCENTRE [11] is analysed in this study. This is a retrofitted building (Figure 3), whose diaphragms had been strengthened with a layer of diagonal timber boards nailed to the original single straight sheathing.

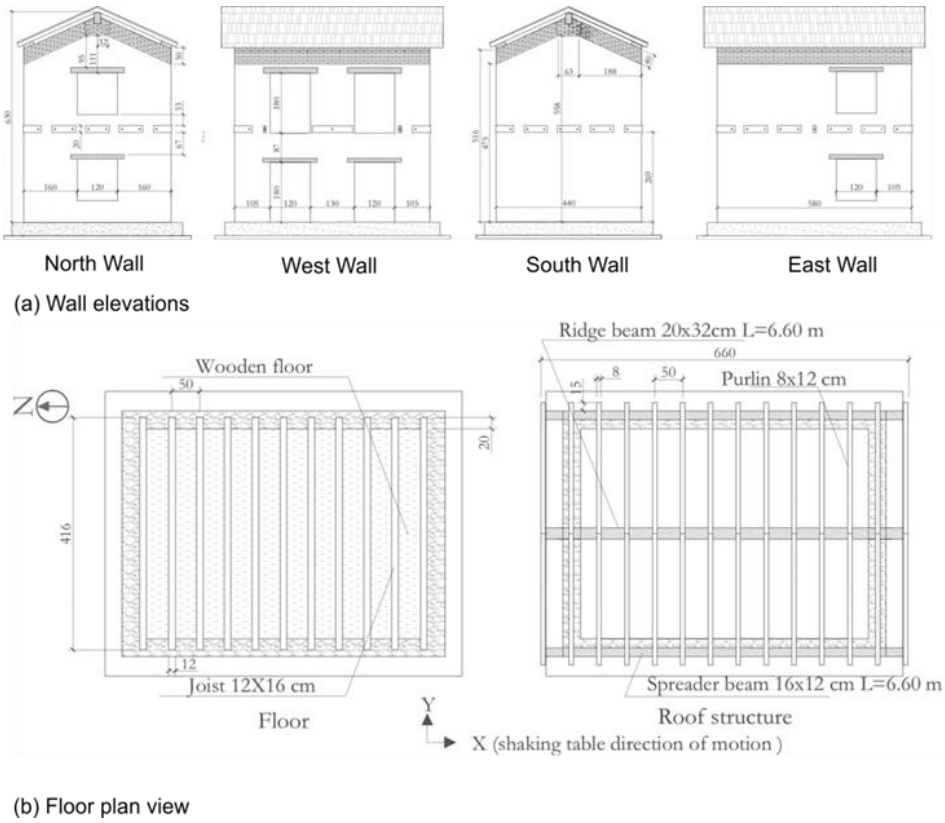

Figure 3: Construction details of tested building, dimensions in cm [11].

In addition, the connections between the floor/roof diaphragms and the walls were also strengthened. At the floor level, 140 mm x 140 mm x 10 mm steel sections were attached to the interior faces of the walls, and bolted through the thickness of the wall using 14mm diameter threaded bars. At the roof level, a continuously reinforced masonry ring beam was constructed using solid brick exterior layers and a cement grouted core. Two 12mm or 16mm diameter longitudinal reinforcements were placed in the central core, with horizontal truss reinforcements connecting the two brick faces at each bed joint. These strengthening measures ensured the global building behaviour to take place, while still allowing some level of diaphragm flexibility.

The building was tested under shake table excitations using the motions of the 15 April 1979 Montenegro earthquake measured at the Ulcinj-Hotel Albatros station with some scaling (Figure 4). The nominal peak ground acceleration (PGA) was gradually increased from 0.05g to 0.7g, for which the actual acceleration (peak) of the table motion varied from 0.06g to 1.16g. In this paper, the excitation levels are referred to by the nominal PGA.

The building suffered some damage during its transportation to the testing facility. Thus, the initial stiffness of the building would have been smaller than if the building had remained undamaged at the start of testing. The response of the building was almost elastic up until the 0.5g excitation. Significant cracking appeared during the 0.6g test sequence, followed by the near-collapse state with the 0.7g excitation. A detailed description of the response characteristics of the building can be found in [11].

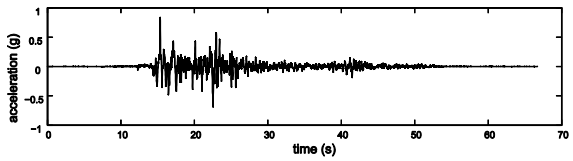

Figure 4: Table acceleration for the 0.6 g test.

MODELLING APPROACH

General Description of the Numerical Model

Figure 5 schematically shows a three-dimensional building model built up as an assemblage of two dimensional components. Each wall is idealised as equivalent plane (2D) frame members consisting of piers and spandrels. These members are connected to nodes (2D wall nodes) at their two ends, with each node having in-plane local degrees of freedom u_{loc}, u_z and ϕ_{rot} (e.g. u_{loc}=u_x for a wall laying in the x-z plane). Three-dimension nodes (3D wall nodes) are used at the intersections of walls, for example at corners of a building, with the global degrees of freedom u_x, u_y, u_z, ϕ_x and ϕ_y. These degrees of freedom are obtained by projecting the local degrees of freedom of the intersecting 2D walls onto the global coordinates. As the contributions of out-of-plane stiffness and strength of a wall are usually small compared to its in-plane stiffness and strength, the out-of-plane degrees of freedoms are neglected. Furthermore, the compatibility of the two intersecting walls is strictly satisfied for the vertical translation, but not for the horizontal translational or the rotational components. This modelling concept allows the direct adoption of the 2D equivalent frame idealisation developed for the individual walls in isolation. In this way, flange effects at wall intersections associated to normal deformations are captured in an approximate way, allowing free warping of the flanged section, whereas no flange effect is captured for shear deformation.

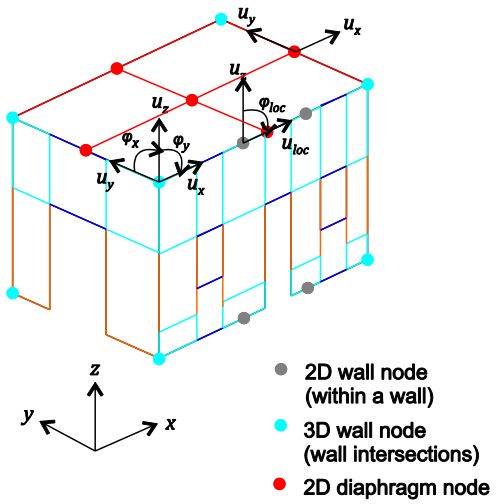

Figure 5: Modelling concept.

The diaphragms are modelled with plane stress or membrane elastic elements where the element node (2D diaphragm node) consists of two in-plane (horizontal) translational degrees of freedom, which permit a linear variation of displacements within an element. These elements are defined by the Young's modulus, shear modulus, and the thickness of the diaphragms. In this study, four elements are used to model a single diaphragm, which is the simplest possible idealisation that can capture the vibration characteristics of the diaphragms.

The masses are assigned by considering simple tributary areas for inertial (horizontal) loading, as shown in Figure 6 and Figure 7 respectively for the floor and wall masses. It should be noted that distributing the mass in this manner does not provide the correct internal force distribution under gravity loading. Thus, additional static nodal forces (vertical forces and moments) are applied in order to obtain the correct gravity forces prior to the dynamic analysis.

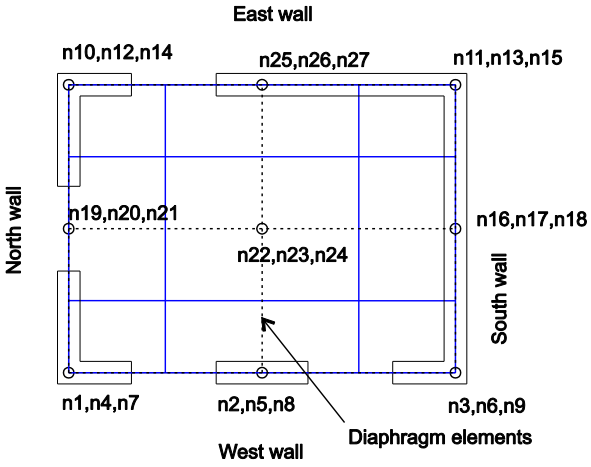

Figure 6: Tributary areas for the distribution of the floor mass.

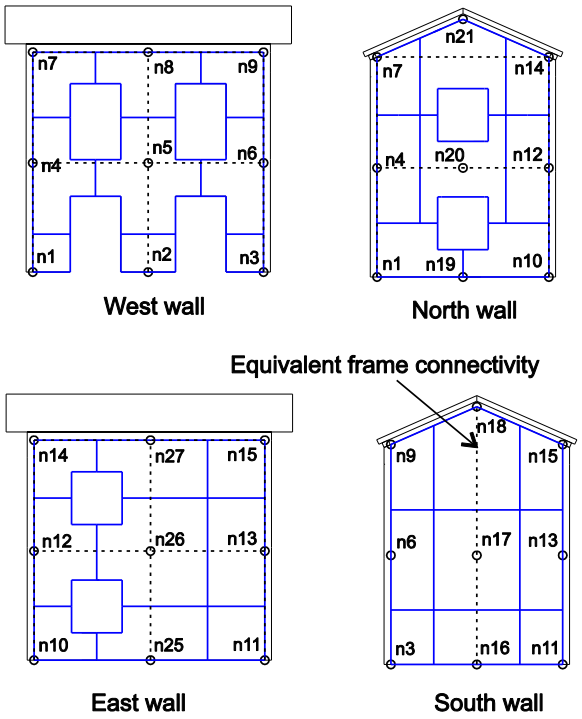

Figure 7: Tributary areas for the distribution of the wall mass.

Limitations of Diaphragm Modelling

The model used for the diaphragms in this study has several limitations, which warrant clarification. Specifically: (1) the diaphragms are considered to be elastic even though actual timber diaphragms can exhibit highly nonlinear material behaviours, (2) full compatibility between the walls and diaphragms is assumed, and (3) only four elements are used to model the diaphragm. These issues are discussed in this section.

Considering the first limitation, even though flexible timber diaphragms can exhibit large deformations, the amount of energy dissipation due to inelastic deformation is usually limited, and the strength degradation is typically not detected for the conceivable range of deformation [12]. For these reasons, the elastic representation of flexible diaphragms in URM buildings can be considered appropriate.

The second assumption related to the full compatibility condition between the walls and diaphragms may not always be appropriate for existing buildings, where floor joists may simply rest within a recess created in the walls without having any strong connection. However, buildings with such poor connections tend to undergo local collapses, before the in-plane wall capacities can be reached. The global building response governed by the in-plane wall resistances can occur only if the wall-diaphragm connections are improved and the local failures are prevented. Hence, assumption of full compatibility between the diaphragms and walls can also be considered as an appropriate simplification when the analysis concerns the global response of the building. Nevertheless, it is possible to include connection flexibility in the stiffness calculation of the diaphragm elements, as suggested by some researchers [13].

The lumped mass modelling of a diaphragm using four membrane elements introduces some inaccuracy. In particular, the peak inertial force of the diaphragm may be reduced to 60% of the more realistic, distributed mass idealisation, due to the smaller effective mass (Appendix A). Despite this discrepancy, lumped mass idealisations have been used successfully in past studies [6, 14]. The reason for this success may be that the discrepancy becomes more significant when the diaphragm flexibility increases, but the natural periods of such flexible diaphragms typically fall in the velocity- or displacement-sensitive region of the response spectra associated with small spectral accelerations, or force demands, compared to those of the stiff masonry walls. Hence, the discrepancy of the lumped mass diaphragm idealisation may not significantly affect the overall computed building responses. In this study, the lumped mass idealisation of the diaphragm is considered to be an acceptable simplification, given the simplified nature of the overall model.

Macroelement Definition

The inelastic behaviours of the piers and spandrels are simulated using the macroelement definition of TREMURI [15]. Each macroelement (pier or spandrel) consists of three segments (Figure 8) with eight in-plane degrees of freedom. The degrees of freedom consists of axial (w_i and w_j) and lateral (u_i and u_j) translations and a rotation (ϕ_i and ϕ_j) at element ends i and j, with two rigid-body displacements defined in the middle segment (w_e and ϕ_i). The top and the bottom interfaces capture the combined axial-rocking interaction and the shear behaviour is concentrated in the middle segment. The axial-rocking behaviour accounts for the limited compressive capacity, while the strength and stiffness degradations occur under shear deformation, as governed by an internal damage parameter. The material properties used in the present analyses (Table 1) were obtained from the results of complementary component tests performed as part of the experimental campaign [16].

Table 1: Masonry material properties from component tests.

Young's modulus (MPa)	Shear modulus (MPa)	Compressive strength f_m (MPa)	Cohesion f_{v0} (MPa)	Friction coefficient μ
2537	841	3.28	0.14	0.14

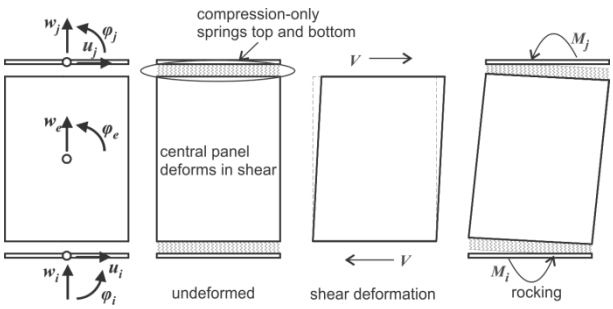

Figure 8: Kinematics of macroelement [15].

Analysis Cases

In order to explore the uncertainties associated with the choice of modelling, four different analysis cases were considered. These cases corresponded to two different idealisations of the equivalent frame definitions, and diaphragm stiffness values calculated using two different approaches.

The two equivalent frame idealisations of the walls oriented in the direction of loading are shown in Figure 9. The first idealisation corresponds to the "full" rigid offsets of the nodes where the rigid zones extend across the full width or the depth of pier and spandrel. The second pattern more accurately reflects the actual crack patterns of the tested building, capturing both the initial damage suffered during the transportation of the building as well as the crack pattern observed from the final stage of testing (reported in a

subsequent section of this paper). The second idealisation was developed considering the following:

- the rigid nodes on the upper storey of the West wall were removed to reflect the cracking occurred during the transportation of the tested building, which separated the reinforced masonry beam from the wall;
- the effective heights of the exterior piers were increased to account for the diagonal crack lines observed in the final run of the test; and
- the thickness of the timber lintels were omitted from the spandrel depth.

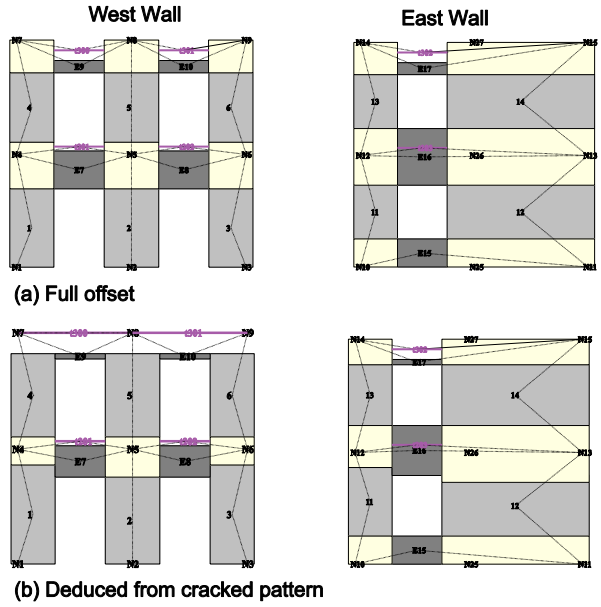

Figure 9: Equivalent frame idealisation of longitudinal walls.

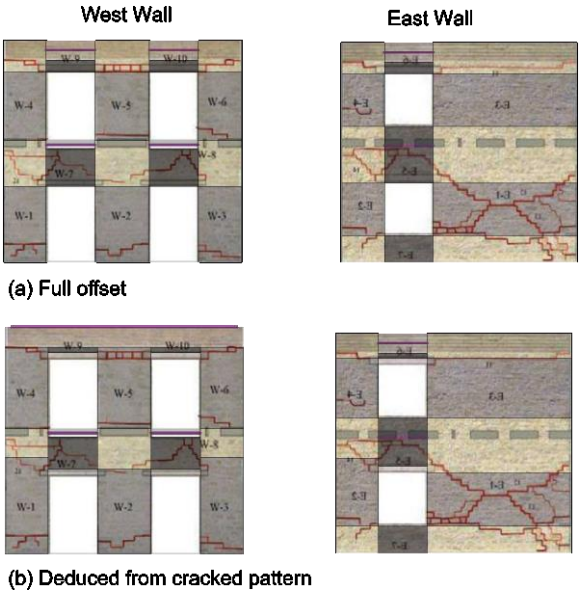

Figure 10: Equivalent frame idealisations superimposed on the final crack patterns.

Figure 10 shows the two equivalent frame idealisation (of Figure 9) superimposed on the final crack patterns observed from the shake table tests. The consideration of the diagonal crack patterns resulted in the increase in the effective (or deformable) heights of the exterior piers of approximately 1.1 to 1.3 times the "full" rigid offset case. In practice, the effective heights reflecting the likely crack patterns may be determined, for example, by making use of assumed 30º crack lines (Figure 1(a)) or by using empirical effective heights derived by Dolce [17].

The two diaphragm stiffness values considered in the present analyses are summarised in Table 2, where the stiffness values (G_d) are defined as the material shear modulus multiplied by the thickness of diaphragm. The first value (D1) corresponds to the expected diaphragm stiffness suggested by ASCE 41-13 [5]. The second stiffness value (D2) was calculated more rigorously using the procedure proposed by Brignola et al. [13], by considering the timber joists to act as flexural beams in parallel. In the latter approach, the interior joists were assumed to be pinned at wall connections, while the end joists were fixed, with the fixity provided by the perimeter steel beams. In addition, the steel beam and the uncracked portion of the masonry wall, as observed from the final test run, were also considered to provide additional stiffness for the floor diaphragm. For the roof diaphragm, the perimeter reinforced masonry beam was included in the stiffness calculation.

The four models analysed were:

- Case 1: full rigid offset with D1
- Case 2: full rigid offset with D2
- Case 3: cracked pattern with D1
- Case 4: cracked pattern with D2

Table 2: Diaphragm stiffness values corresponding to retrofitted floor and roof with large joist cross sections.

Type	Diaphragm stiffness G_d	
	Floor (kN/m)	Roof (kN/m)
D1	3150	3150
D2	7036	5189

ANALYSIS RESULTS AND DISCUSSIONS

The accuracies of the numerical models were assessed by comparing the results predicted by these models with the experimental data in terms of the modal properties (frequencies and mode shapes), peak displacements and the distribution of damage.

The modal properties are presented in Figure 11 and Figure 12 for the experiment and numerical results respectively. The experimental mode properties reported by Magenes et al. [11] were identified from the signal analysis of the ambient and random vibrations with peak table accelerations ranging between ± 0.03g. The mode shapes and frequencies of Figure 11 were obtained prior to the 0.05g test run, and hence represent the initial (elastic) mode properties of the experimentally tested building.

The same number of significant modes in the direction of excitation were identified from the experimental results and the numerical analysis. The fundamental mode of vibration in the direction of excitation is reasonably well captured by all analysis models. It can be seen that the increase in the displacement value up the height of the building is better captured when the diaphragm stiffnesses are calculated using the more refined procedure (Cases 2 and 4). In particular, the closest fundamental mode shape is achieved by Case 4, where the mid-span deformations of the diaphragms relative to the supporting walls are the smallest. In general, the numerical models exhibit larger deformations of the diaphragms relative to the walls, and underestimate the fundamental frequency in comparison to the experimental result.

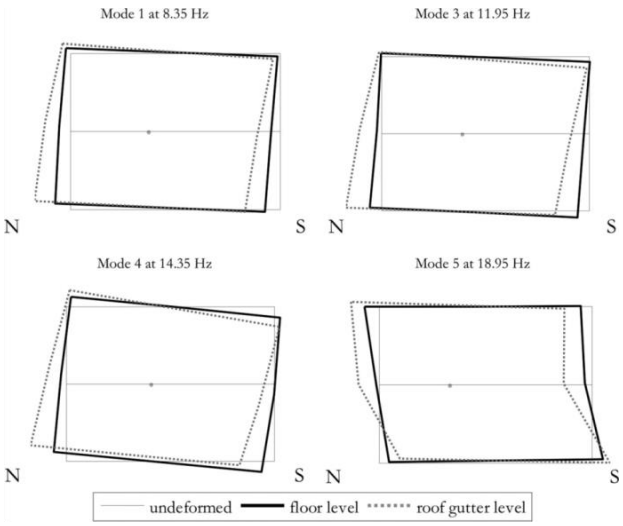

Figure 11: Mode shapes and frequencies identified from ambient and random vibrations [11].

In contrast to the fundamental mode, the displacement shapes of the higher modes are not captured so well. The out-of-phase vibration of the floor and the roof diaphragms is more pronounced in the numerical analysis compared to that observed experimentally (2nd significant mode). The 3rd experimentally observed mode resembling the rotation of the diaphragms as a rigid-body could not be identified by the numerical models. The highest significant mode shape found in the experiment appears to be a mixture of the two highest modes predicted by the numerical models.

The larger diaphragm displacements and the reduced torsional rotation are due to the lack of coupling between the diaphragms at adjacent levels, as well as a lack of coupling between diaphragms and the in-plane loaded walls. This coupling is provided by the out-of-plane deformations of walls, which were neglected in the analysis. The implication is that the out-of-plane walls may play an important role (particularly if the height-to-thickness ratio of the wall is not large, as in the tested building), at least within the elastic range of the building response.

The notion that the out-of-plane walls affect the elastic building response can also be inferred from the normalised Fourier amplitudes of displacements calculated at the diaphragm mid-spans (Figure 13). For the 0.4g excitation (when the building remains almost elastic), the numerical analyses show large responses occurring near 10 Hz, which corresponds to the natural frequency of the diaphragm. In contrast, the experimental data do not show significant peaks corresponding to those frequencies. This discrepancy may be due to the out-of-plane motions of walls, which act to "restrain" the independent motions of the diaphragms.

The importance of the out-of-plane loaded walls to the global building response appears to become less significant as the building becomes inelastic, which is reflected in the form of increased consistency of the Fourier amplitude for the 0.6g excitation. However, Figure 13 shows that this increased consistency is due to the reduced diaphragm motion as the in-plane loaded walls become inelastic, and may not necessarily be due to the reduced effect of the out-of-plane responding walls. Nevertheless, neglecting the out-of-plane wall appears to be generally more appropriate in the inelastic range of the building response.

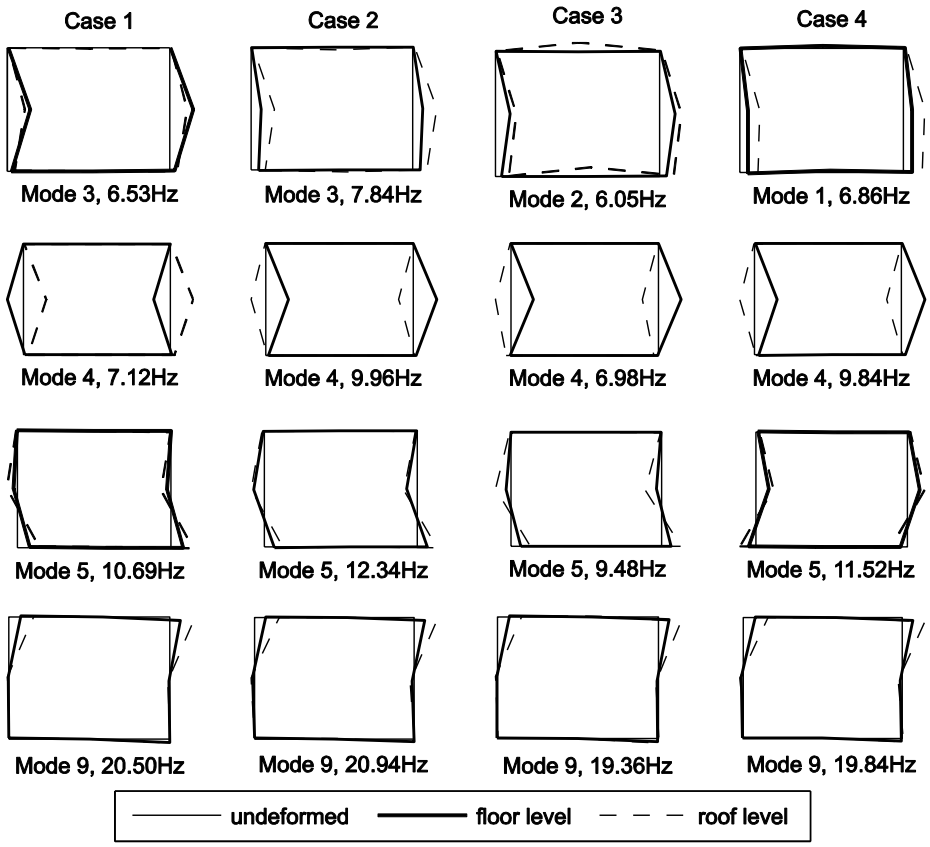

Figure 12: Significant mode shapes and frequencies from numerical analysis.

The peak displacement envelopes found experimentally, as well as numerically, are compared in Figure 14 for the West and East walls as well as at the diaphragm mid-spans. The results corresponding to 0.4g, 0.5g, 0.6g and 0.7g excitation intensities are shown for the four analysis cases. The general trends of the experimental results show that the peak displacements of the walls and the diaphragms approach towards each other as the excitation intensity increases. This trend is captured by all numerical models also. In general, the sensitivity of the analysis to the diaphragm stiffness is small, although the elastic response (0.4g and 0.5g intensities) is affected to some degree. The discretisation of the equivalent frame appears to have more importance. The upper storey displacements of the West wall are better captured by Cases 3 and 4 in the elastic range, implying that the equivalent frame idealisation based on the cracked pattern provides a better correlation with the experimental data. However, when significant inelastic response occurs during the 0.7g excitations, no significant differences of these responses predicted by the four different models are found, and all models exhibit soft-storey behaviour with damage concentration in the ground storey.

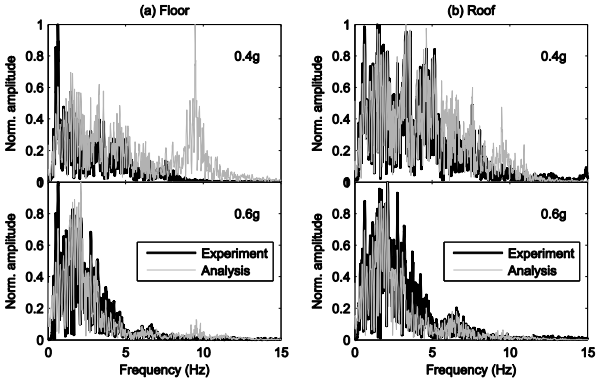

Figure 13: Normalised Fourier amplitudes of displacements at (a) floor mid-span, (b) roof mid-span for Case 4.

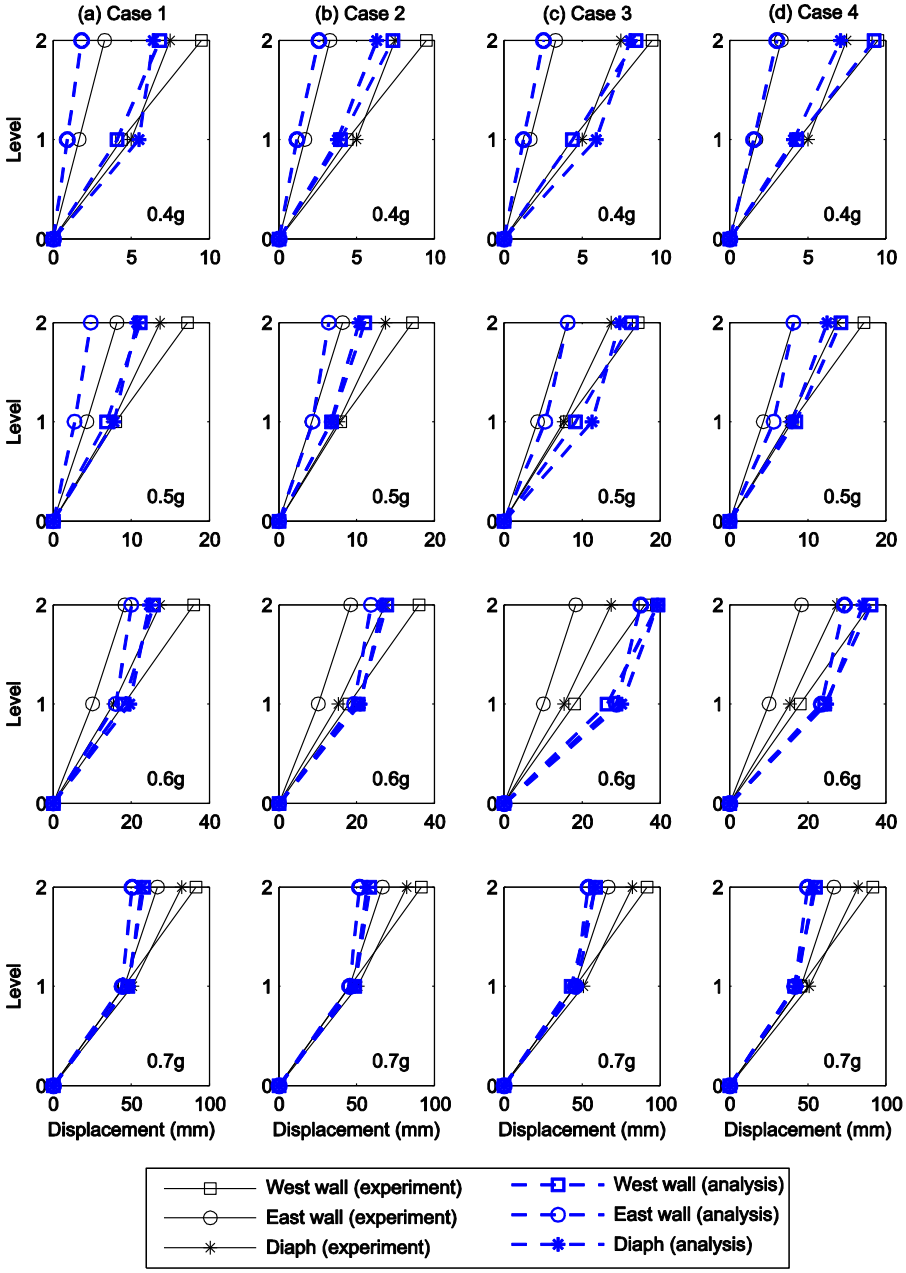

Figure 14: Comparisons of peak displacement envelopes.

The distribution of damage is assessed using the ratios between the rotations due to rocking and drifts due to shear (δ_b and δ_s) and their corresponding ultimate capacities ($\delta_{b,ult}$ and $\delta_{s,ult}$) for a given macroelement. The rocking rotations and shear drifts are expressed as the flexural and the shear components of chord rotation [15] (Figure 8), which may be expressed as

$$\delta_b = \frac{\phi_i + \phi_j}{2} + \phi_e \quad (1)$$

$$\delta_s = \frac{u_j - u_i}{h} + \phi_e \quad (2)$$

where h is the deformable height of the pier or length of the spandrel. The definitions of the other variables are given in Figure 8.

The ultimate rocking and drift capacities obtained from the component tests [16] were $\delta_{b,ult}$ = 0.6 % and $\delta_{s,ult}$= 0.3 %, which were used in the present study. These values corresponded to the deformations of the statically tested piers when the lateral resistance reduced to 80% of the peak value. The damage ratios are hence defined as $DL_b = \delta_b/\delta_{b,ult}$ and $DL_s = \delta_s/\delta_{s,ult}$ for rocking and shear respectively. Ratios greater than 1 indicate the notional failure of that component under the considered failure mechanism for the purpose of seismic assessment.

The damage ratios estimated for the 0.6g and 0.7g excitations are compared against the experimental crack patterns in Figures 15 and 16 respectively. The top and bottom values for each element of the figures indicate DL_b and DL_s, respectively. Results for the analysis Cases 2 and 4 are shown, and where the damage ratios exceed 1, indicative failure patterns are also shown in grey (straight lines at the element ends indicate the rocking failure, and the diagonal lines across the element indicate the shear failure). For the 0.6g excitation intensity, the analysis based on Case 4 predicted rocking-dominant behaviour of the West wall, which is consistent with the experimental observation. In contrast, Case 2 predicted predominant shear damage. Hence, the damage mechanism is also better captured when the equivalent frame idealisation is based on the actual crack patterns. For the 0.7g excitation, however, both models show qualitatively identical damage distribution, which indicated that they generated almost identical displacements. At this near-collapse state, however, the predicted failure patterns are not in good agreement with the experimental results. In particular, for the West wall, the numerical analysis shows a failure governed by shear damage, while the experimental crack patterns actually indicate predominantly rocking failure.

Comparing the peak displacement shapes (Figure 14) and the damage distributions for the 0.7g excitation, the rocking responses of the upper storey piers of the West wall are found to be generally underestimated by the numerical analyses. A number of variations of the material properties were investigated with the aim of achieving larger upper storey (rocking) deformations for the final test run. However, in all simulations, initial flexural-rocking behaviour of the bottom storey piers was followed by significant shear damage. Once shear damage occurred, the models underwent soft-storey collapse, and the increased deformation of the upper-storey could not be attained. To some extent, this outcome may be considered as the limitation of the equivalent frame approach in capturing the dynamics of extensively damaged URM buildings.

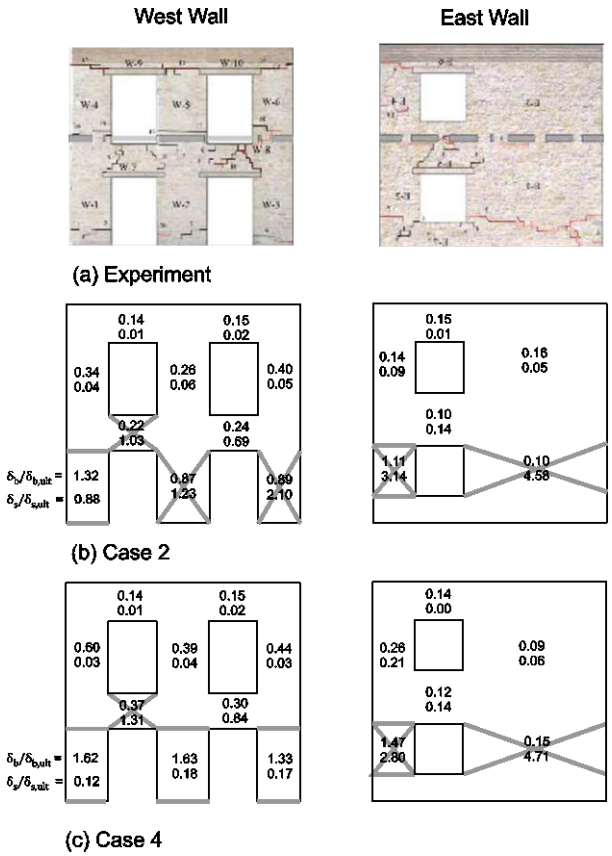

Figure 15: Comparison of (a) experimental crack patterns, (b) damage ratios predicted by Case 2, and (c) damage ratios predicted by Case4, for 0.6 g excitation.

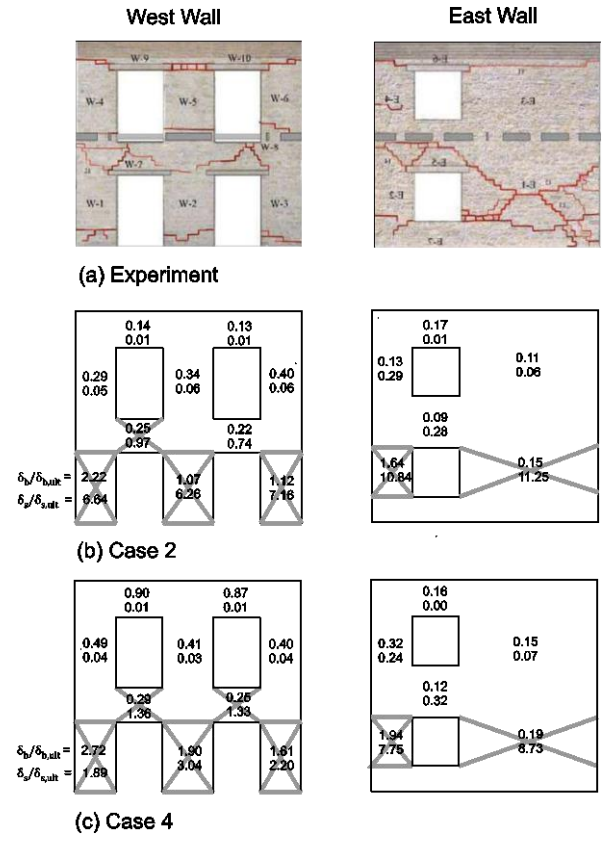

Figure 16: Comparison of (a) experimental crack patterns, (b) damage ratios predicted by Case 2, and (c) damage ratios predicted by Case 4, for 0.7 g excitation.

INFLUENCE OF DIAPHRAGM FLEXIBILITY

The sensitivity of the building response due to relatively large diaphragm flexibility was investigated numerically. Using the analysis Case 4, the stiffnesses of the floor and the roof diaphragms were reduced from their original values (D2 in Table 2) to 0.005 times these original values. The stiffness value of 0.005 times the original values is likely to be unrealistically low for the test building, but were analysed to observe the general trends of the responses. Figure 17 shows the peak displacement variations of the West and the East walls at the roof level (u^r_{west} and u^r_{east} respectively) as well as the peak deformation of the roof diaphragm mid-span relative to the walls (Δ^r_d). Note that Δ^r_d is the diaphragm displacement relative to the average displacements of the in-plane loaded walls, and not to the ground. The peak deformations of the floor diaphragm showed similar trends to those of the roof diaphragm and are not shown for clarity. The results correspond to the 0.6g excitation, and are plotted against the average diaphragm period (T_d) of the floor and the roof (the two diaphragms had almost identical period values). The diaphragm periods approximately corresponding to the diaphragm stiffness D1 (Table 2) and the lower-bound stiffness suggested by ASCE 41-13 [5], which represents single straight sheathing diaphragms of the test building, are also indicated. It can be observed that the diaphragm flexibility has significant effects on the seismic demands of the in-plane response of walls. In particular, for the West wall, which is more flexible, a displacement amplification of 220% is observed between the as-built diaphragm D2 and the lower-bound stiffness values.

Such amplification is due to two factors associated with flexible diaphragms; namely, (1) the variation of the diaphragms' inertial forces and (2) reduced coupling between the walls when the diaphragms are flexible. The effect of the first factor can be seen in Figure 18, where the spectral acceleration of the 0.6g table motion is plotted with respect to the diaphragm periods (normalised with respect to values corresponding to the original diaphragm). The comparison between the spectral accelerations and the peak wall displacements (Figure 17) indicates that the wall displacement amplifications occur when the spectral accelerations (or inertial forces) of the diaphragms are amplified. Once the spectral acceleration is reduced for T_d greater than approximately 0.7 s, the peak wall displacement is also reduced. The peak inertial force of the diaphragm hence directly affects the displacement demands of the walls. This observation also implies that the amplification is dependent on the ground motion characteristics. The second factor exacerbates the amplification of the weaker/flexible side (i.e. West wall) due to the limited coupling provided by flexible diaphragms in redistributing the internal forces.

It can be seen that the peak diaphragm deformation (Figure 17) closely reflects the spectral displacement (Figure 18), suggesting that the diaphragm deformation may be estimated directly from the elastic spectrum. The similarity occurs because the diaphragms are modelled as being elastic, and the in-plane loaded walls are generally much stiffer than the diaphragms. Hence, the diaphragms essentially behave as elastic single-degree-of-freedom systems with rigid supports. When the diaphragms are relatively stiff (and the walls can no longer be considered as rigid supports), some deviations can be seen between the peak diaphragm deformations and the elastic displacement spectrum.

Even though the diaphragm deformation may be approximated by the spectral displacement, it is questionable if the diaphragm deformation actually matches the displacement spectrum when the diaphragm is overly flexible, without causing instability of the out-of-plane responding walls. Further studies are needed to investigate the effect of the dynamic response of the out-of-plane walls (particularly for the two-way spaning walls) on the building response when the diaphragm becomes excessively flexible.

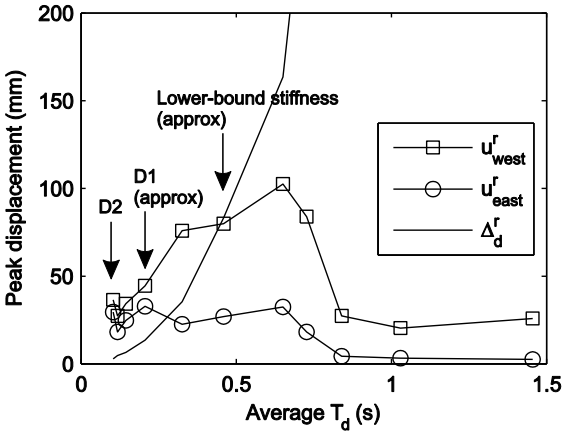

Figure 17: Influence of diaphragm stiffness on the wall displacement and roof deformation, subjected to the 0.6 g excitation intensity.

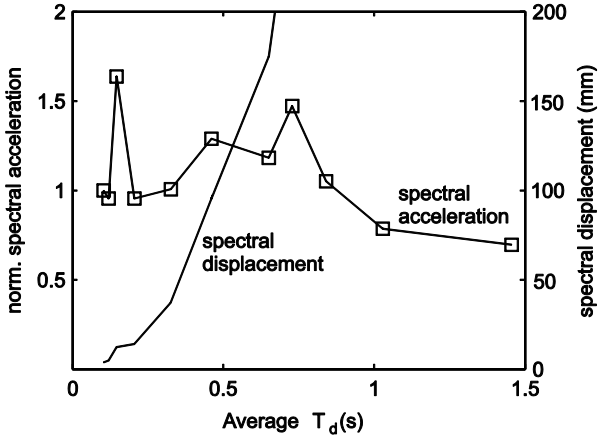

Figure 18: Plots of normalised spectral acceleration and displacement corresponding to the average diaphragm period for the 0.6 g excitation.

CONCLUSIONS

In this paper, results of a case study are reported on the applicability of the equivalent frame modelling approach for the global analysis of URM buildings with flexible diaphragms, when the local out-of-plane failure mechanisms have been mitigated. Reflecting the current modelling practice, the diaphragms were considered to remain elastic and the out-of-plane wall stiffness and strength contributions were neglected.

The simple modelling approach was able to capture, with reasonable accuracy, the fundamental mode characteristics and the evolution of the peak displacements as the excitation intensity increased. On the other hand, the higher modes and the damage mechanisms were not as accurately simulated, particularly towards the near-collapse state.

Concerning the damage mechanisms, different failure mechanisms were obtained (prior to the ultimate state) depending on the assumed length of the rigid node offset. More consistent results (with respect to the experimental data) were achieved when the equivalent frame idealisation reflected the actual crack pattern.

For the case study building, the analyses did not indicate large sensitivity to the diaphragm stiffness values. When the diaphragms were made relatively flexible, however, the

numerical models indicated the potential for significant sensitivity, including amplification, of the wall displacements due to the diaphragm stiffness values.

The analyses also revealed that perhaps the most significant limitation of the investigated modelling approach is the omission of the out-of-plane walls. The discrepancies in the mode properties were identified as primarily due to the lack of out-of-plane wall stiffness. The interaction between the out-of-plane responding wall and flexible diaphragm is also expected to play an important role as the diaphragm flexibility increases.

Considering these points, the following conclusions can be drawn for practical application:

- The analyses are sensitive to the frame geometry (deformable lengths of piers) and the best agreement with the actual response is expected when the geometry is guided by the crack pattern. Clearly, when the frame model is used for prediction of the response, the final crack pattern may not be obvious, in which case the engineer may need to consider the sensitivity of the results by varying the length of the piers. In such sensitivity analysis, an absolute minimum deformable length of the frame should correspond to height of the adjacent openings. In addition, any pre-existing crack should be reflected in the idealisation;
- Neglecting out-of-plane loaded walls may render the results inaccurate if the diaphragm deformation is significant, and/or the building response is predominantly elastic;
- If diaphragm stiffness is known, then the likely level of diaphragm deformation (relative to the supporting walls) may be gauged from the elastic displacement spectrum as a preliminary consideration;
- If the diaphragm deformation is deemed to be excessively large, alternative analysis approaches that can account for two-way spanning out-of-plane wall behaviour, such as the finite element method, may be warranted; and
- If diaphragm stiffness is unknown, a sensitivity analysis on the stiffness value is recommended due to the relatively flexible diaphragms significantly affecting the wall displacement demand.

ACKNOWLEDGEMENTS

This work was supported by the Australian Research Council, through the grant DP120100848. The first author received financial support through the Australian Postgraduate Award. The authors would like to thank Prof. Magenes, Asst. Prof. Penna and Dr. Senaldi from the University of Pavia and EUCENTRE for their suggestions on the numerical modelling of the experimentally tested building. The authors would also like to thank Prof. Magenes for reviewing the original manuscript.

REFERENCES

1 Magenes G and Della Fontana A (1998). "Simplified non-linear seismic analysis of masonry buildings". *Proc. of the British Masonry Society*, **8**. 190-195.

2 Kappos AJ, Penelis GG and Drakopoulos CG (2002). "Evaluation of simplified models for lateral load analysis of unreinforced masonry buildings". *Journal of Structural Engineering*, **128**(7). 890-897.

3 Salonikios T, Karakostas C, Lekidis V and Anthoine A (2003). "Comparative inelastic pushover analysis of masonry frames". *Engineering Structures*, **25**. 1515-1523.

4 Lagomarsino S, Penna A, Galasco A and Cattari S (2013). "TREMURI program: An equivalent frame model for the nonlinear seismic analysis of masonry buildings". *Engineering Structures*, **56**. 1787-1799.

5 American Society of Civil Engineers (2014). "*Seismic evaluation and retrofit of existing buildings".* ASCE/SEI 41-13, American Society of Civil Engineers, Reston, Virginia, 518 pp.

6 Tena-Colunga A and Abrams DP (1992). "*Response of an unreinforced masonry building during the Loma Prieta earthquake"*. Structural Research Series 576, Department of Civil Engineering, University of Illinois at Urbana-Champaign, 288 pp.

7 Costley AC and Abrams DP (1995) "*Dynamic response of unreinforced masonry buildings with flexible diaphragms*". Structural Research Series 605, Department of Civil Engineering, University of Illinois at Urbana-Champaign, 281 pp.

8 Dizhur D, Ingham JM, Moon L, Griffith MC, Schultz A, Senaldi I, Magenes G, Dickie J, Lissel S, Centeno J, Ventura C, Leite J and Lourenço P (2011). "Performance of masonry buildings and churches in the 22 February 2011 Christchurch earthquake". *Bulletin of New Zealand Society for Earthquake Engineering*, **44**(4). 279-296.

9 Aleman J, Mosqueda G and Whittaker A (2015). "*Seismic analysis of multi-story unreinforced masonry buildings with flexible diaphragms"*. MCEER Report-15-0001, University of Buffalo, State University of New York, 407 pp.

10 Derakhshan H, Griffith MC and Ingham JM (2015). "Out-of-plane seismic response of vertically spanning unreinforced masonry walls connected to flexible diaphragms". *Earthquake Engineering and Structural Dynamics*. In Press. DOI: 10.1002/eqe.2671.

11 Magenes G, Penna A, Senaldi I, Rota M and Galasco A (2014). "Shaking table test of a strengthened full-scale stone masonry building with flexible diaphragms". *International Journal of Architectural Heritage: Conservation, analysis and restoration*, **8**(3). 349-375.

12 Giongo I, Wilson A, Dizhur D, Derakhshan H, Tomasi R, Griffith M, Quenneville P and Ingham JM (2014). "Detailed seismic assessment and improvement procedure for vintage flexible timber diaphragms". *Bulletin of New Zealand Society for Earthquake Engineering*, **47**(2). 97-118.

13 Bringola A, Pampanin S and Podesta S (2012). "Experimental evaluation of the in-plane stiffness of timber diaphragms". *Earthquake Spectra*. **28**(4). 1687-1709.

14 Kim S-C and White DW (2004). "Nonlinear analysis of a one-story low-rise masonry building with a flexible diaphragm subjected to seismic excitation". *Engineering Structures*, **26**. 2053 - 2067.

15 Penna A, Lagomarsino S and Galasco A (2014). "A nonlinear macroelement model for the seismic analysis of masonry buildings". *Earthquake Engineering and Structural Dynamics*, **43**(2). 159-179.

16 Magenes G, Penna A, Galasco A and Da Paré M (2010). "In-plane cyclic shear tests of undressed double-leaf stone masonry panels". *Proceedings of 8th International Masonry Conference* (8IMC), Dresden, Germany, July 4 – 7, Paper No 216.

17 Dolce M (1989). "Schematizzazione e modellazione degli edifice in muratura sogetti ad azioni sismiche (Modelling of masonry buildings under seismic loads)". *L'industria delle Construzioni*, **242**. 44-57. (in Italian).

18 Wilson A, Quenneville P and Ingham JM (2013). "Natural period and seismic idealization of flexible timber diaphragms". *Earthquake Spectra*, **29**(3). 1003-1019.

19 Chopra A (2007) "*Dynamics of Structures - theory and application to earthquake engineering*". 3rd Edition, Prentice Hall, New Jersey, 876 pp.

20 Standards Australia (2007). "*AS 1170.4 - 2007: Structural design actions. Part 4: Earthquake actions in Australia*". Standards Australia, Sydney, 52 pp.

APPENDIX A

The lumped mass idealisation of the diaphragm introduces some inaccuracies, in particular, concerning the forces generated by the diaphragm motion. Two idealised elastic diaphragm models are analysed to illustrate this point, considering the supporting in-plane walls to be rigid. The first model corresponds to a generalised SDOF system of a shear beam with uniformly distributed mass, assuming the displacement shape, ψ, to be the deformed shape of the beam subjected to a parabolic load. This model may be considered to be representative of actual timber diaphragms [18]. The generalised mass $\tilde{m}$, generalised stiffness $\tilde{k}$ and the period T of the system are

$$\tilde{m} = \frac{3968}{7875}m \ , \qquad \tilde{k} = \frac{4352}{875}\frac{GA}{\kappa L} \ , \quad T = 2\pi\sqrt{\frac{\tilde{m}}{\tilde{k}}} \tag{A1}$$

where m is the total mass of the diaphragm including the contributions from out-of-plane walls, G is the shear modulus, A is the diaphragm cross section area, L is the span length and κ is the cross section shape factor for shear.

The peak displacement at mid-span u_0 and the peak elastic restoring force V_0 of the shear beam are given by [19]

$$u_0 = \tilde{\Gamma}D, \qquad V_0 = \tilde{\Gamma}\tilde{L}A \tag{A2}$$

where $\tilde{L} = \int_0^L \bar{m}\psi dx$, with $\bar{m}$ =mass per unit length, and $\tilde{\Gamma} = \tilde{L}/\tilde{m}$. D and A express the peak displacement and pseudo-acceleration correspondingly.

The equivalent mass and the stiffness corresponding to the lumped mass idealisation of the diaphragm used in this study are

$$\tilde{m} = \frac{1}{2}m \ , \qquad \tilde{k} = 4\frac{GA}{\kappa L} \tag{A3}$$

The peak mid-span displacement and the base shear force of the lumped mass system are

$$u_0 = D, \qquad V_0 = \tilde{m}A \tag{A4}$$

Figures A1 show the comparisons of the period, peak mid-span displacement and the peak elastic restoring force obtained from the two idealisations, subjected to the design spectrum of AS 1170.4 [20] with a peak ground acceleration of 0.1g on site class C_e. The diaphragm stiffness G_d, defined as the shear modulus multiplied by the thickness, was set to 1750kN/m (approximately representing a diaphragm with double layered sheathing [5]), and results correspond to the span length of 10 m and several different aspect ratios (L/B). It can be seen that both the periods and the peak displacements of the two idealisations match well. However, the elastic force demand of the lumped mass model is consistently smaller than the generalised SDOF idealisation of the distributed mass model. This discrepancy is mainly attributed to the difference in the "effective" mass of the two models. For the generalised SDOF shear beam, the "effective" mass, which produces the peak base shear when multiplied by the spectral acceleration, is equal to $\tilde{\Gamma}\tilde{L} = 0.815m$ (from Eq. A2). For the lumped mass idealisation, the corresponding value is $\tilde{m} = 0.5m$ (from Eq. A4). Hence the peak elastic force imposed on the lumped mass idealisation is approximately 60% of the more representative, shear beam model with distributed mass.

Despite the theoretical discrepancy, the lumped mass idealisation has been used successfully in past studies [6,14]. The reason may be that the discrepancy is most significant when the diaphragm is relatively flexible. For stiff diaphragms, the wall supports do not remain rigid, and the participation of the wall mass will likely reduce the discrepancy. Indeed, at the limiting condition of a rigid diaphragm, the two idealisations will yield identical results, as governed by the total mass of the diaphragm and the stiffness of the walls. Hence the lumped mass model is expected to be appropriate when the diaphragm is relatively stiff, while it can underestimate the force demand by up to 40% when the diaphragm becomes overly flexible. However, for such flexible diaphragms the force demands are also usually small, and hence, may have only limited effects on the building response. In this study, lumped mass idealisation is considered to be an acceptable simplification, given the simplified nature of the overall model.

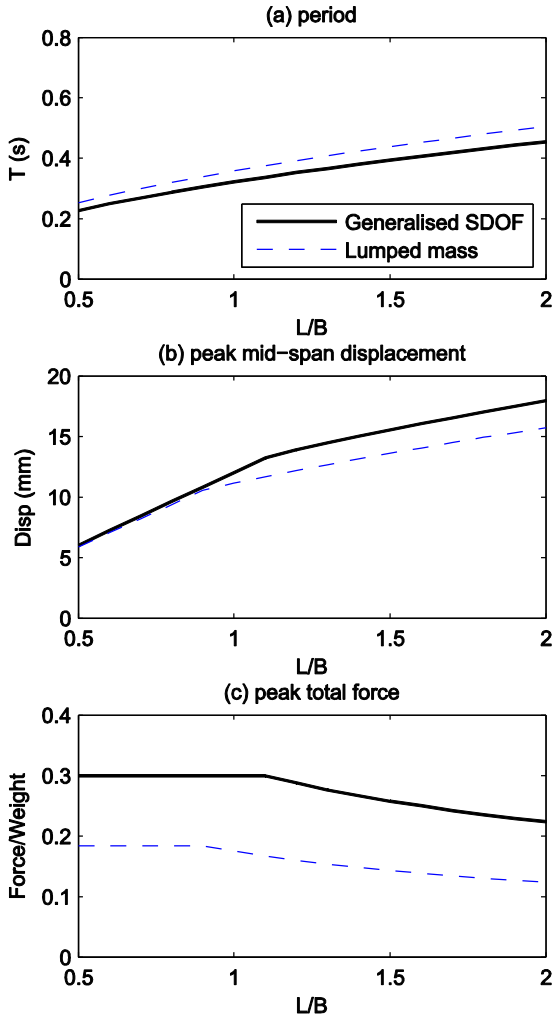

Figure A1: Comparisons of (a) period, (b) peak mid-span displacement, and (c) peak base shear of the diaphragm idealisations. L is the span length and B is the width of the diaphragm.